

PAPER

## Detection of moisture content profile of concrete using ground penetrating radar

To cite this article: Zihan Xia *et al* 2025 *Eng. Res. Express* **7** 015119

View the [article online](#) for updates and enhancements.

### You may also like

- [Numerical investigation of indirect parallel PVT solar systems using MATLAB/simulink](#)  
Sirine Saidi, Taoufik Brahim and Abdelmajid Jemni
- [Assessment of strength enhancement and structural performance in fiber-reinforced concrete with varying fiber types and percentages](#)  
Neeti Mishra, Rajendra Kumar Srivastava and Rakesh Varma
- [A new approach utilizing DTCWT for feature extraction and ANN for classification to improve fingerprint recognition](#)  
Pradeep N R, Manjunatha D V, Napoleon A et al.

# Engineering Research Express



## PAPER

# Detection of moisture content profile of concrete using ground penetrating radar

RECEIVED  
21 November 2024

REVISED  
17 December 2024

ACCEPTED FOR PUBLICATION  
24 January 2025

PUBLISHED  
11 February 2025

Zihan Xia<sup>1</sup> , Liyu Xie<sup>1,2</sup> , Songtao Xue<sup>1,2,3</sup> and Peng Zhu<sup>4,\*</sup> 

<sup>1</sup> Department of Disaster Mitigation for Structures, Tongji University, Shanghai, People's Republic of China

<sup>2</sup> State Key Laboratory of Disaster Reduction in Civil Engineering, People's Republic of China

<sup>3</sup> Department of Architecture, Tohoku Institute of Technology, Sendai, Japan

<sup>4</sup> Department of Structural Engineering, Tongji University, Shanghai, People's Republic of China

\* Author to whom any correspondence should be addressed.

E-mail: [xzhoo@tongji.edu.cn](mailto:xzhoo@tongji.edu.cn), [liyuxie@tongji.edu.cn](mailto:liyuxie@tongji.edu.cn), [xue@tongji.edu.cn](mailto:xue@tongji.edu.cn) and [pzhu@tongji.edu.cn](mailto:pzhu@tongji.edu.cn)

**Keywords:** GPR, moisture content profile, FWI, concrete, non-contact monitoring

## Abstract

Moisture content in concrete is essential, as it influences durability, strength, and cracking susceptibility, critical for structural longevity and safety. This paper aims to explore the potential of GPR in detecting the distribution of moisture content in concrete. By utilizing the approximate linear relationship between the dielectric constant and the moisture content of concrete, this study realizes the detection of concrete moisture content profile by GPR. The concrete moisture content profile is derived from radar echo data using full waveform inversion (FWI). The simulations show that different initial values converge to the true values with a maximum error of 0.33%, demonstrating the feasibility of the method. Experimental results demonstrate a strong correlation between GPR measurements and the gravimetric method, with an average error of 2.5%, affirming the accuracy of GPR in detecting moisture content profiles for engineering applications.

## 1. Introduction

Concrete is the most popular building material today. In the past few decades, it has been widely used in constructing houses, factories, commercial buildings, bridges, tunnels and other infrastructure (Neville, 1995, Shetty and Jain 2019, Li *et al* 2022). The moisture content of concrete is a crucial parameter closely related to construction quality, progress, and security. In construction quality control, researchers have utilized ground penetrating radar (GPR) to monitor variations in concrete moisture content, enabling the assessment of the setting state of the concrete (Prego *et al* 2016, Xie *et al* 2022). Construction schedule management enables schedule modifications by comparing the predicted concrete moisture content profiles at different construction phases with the moisture content profile detection (Ghodoosi *et al* 2018). Furthermore, high moisture content leads to a decrease in the strength of concrete. The hidden danger areas can be located by detecting the high moisture content areas of the concrete moisture content profile in construction security assessment (Fernandes *et al* 2017, Klewe *et al* 2021).

Researchers have proposed several methods to determine the moisture content of concrete since it plays a significant role in engineering. Various concrete moisture content detection methods are summarized and compared in table 1. Current methods for measuring moisture content exhibit various strengths and limitations. Techniques such as the gravity method and nuclear magnetic resonance are significantly constrained by their lack of non-destructive and *in situ* detection capabilities. While neutron radiography and x-ray imaging offer non-destructive testing, their practical application is hindered by safety concerns and the high cost of equipment. Patch antennas are economical and convenient but have limited applicability across diverse scenarios. In contrast, GPR stands out for its non-destructive nature, *in situ* detection capability, and high safety standards, demonstrating superior versatility and reliability for moisture content measurement across a wide range of applications.

**Table 1.** Comparison of detection methods.

Detection method	Non-destructive	<i>In-situ</i>	Security	Equip cost (\$)
Gravity method	×	×	✓	2~20
Neutron radiography (Moradillo <i>et al</i> 2019)	✓	×	×	5 000~30 000
Nuclear magnetic resonance (Wang <i>et al</i> 2017)	×	×	×	4 000~200 000
X-ray (du Plessis and Boshoff 2019, Sugiyama and Promentilla 2021)	✓	×	×	6 000~20 000
Patch antenna (Xue <i>et al</i> 2021, Yi <i>et al</i> 2023)	✓	×	✓	20~100
GPR (Laurens <i>et al</i> 2005, Kaplanvural <i>et al</i> 2018, Xie <i>et al</i> 2022)	✓	✓	✓	3 000~30 000

Due to the susceptibility of electromagnetic waves to water, numerous scholarly investigations have been undertaken to examine the relationship between the characteristics of GPR data and the moisture content. Based on the uniformity assumption, Agred *et al* calculated the average moisture content in concrete using the propagation velocity of electromagnetic waves (Agred *et al* 2018). Subsequently, Dinh *et al* also found that water and chloride ions will attenuate the propagation of electromagnetic waves in pavement evaluation, indicating that the reflection coefficient of the impedance mismatch layer can be used to determine the moisture content of each pavement layer (Dinh *et al* 2016). However, the qualitative results based on the uniformity assumption can only be used as a preliminary assessment in engineering, which also greatly limits the application of GPR. Besides, the uniformity assumption is inconsistent with the reality of the non-uniform distribution of moisture content. Therefore, the uniformity assumption in GPR detection needs to be improved and optimized.

In order to apply GPR to concrete moisture content profile detection in engineering, it is necessary to consider the non-uniform distribution of moisture content in concrete to realize the quantitative evaluation of concrete moisture content. Hugenschmidt and Loser investigated the impact of moisture and chloride content on the radar signal reflection amplitude. A qualitative assessment of moisture and chloride variations in concrete by utilizing the ratio of reflected signals from the concrete surface and aluminum foil is proposed (Hugenschmidt and Loser 2008). Building upon this, researcher separately developed empirical formulas for the electrical conductivity of saturated concrete in relation to chloride ions, and for the dielectric constant of saturated concrete in relation to moisture content (Kalogeropoulos 2012). However, wave velocity and reflection coefficient methods face limitations in accurately assessing moisture content in non-uniformly distributed environments. Voigt *et al* and Sun highlighted that wave velocity measurements can produce significant errors in concrete with variable moisture distributions. In regions with substantial density and porosity differences, changes in wave velocity may lead to misleading moisture estimates (Voigt *et al* 2006). Similarly, Huisman *et al* found that reflection coefficients become unstable with humidity fluctuations, especially in high-moisture or complex conditions, where factors like pore structure and material composition affect signal accuracy (Huisman *et al* 2003). Joshaghani and Shokrabadi further noted that while reflection coefficients indicate moisture presence, they offer limited precision in quantitative measurement, especially when moisture variations are minimal (Joshaghani and Shokrabadi 2022). The structure of concrete is complex and variable, with differing pore structures, material compositions, and densities, making accurate moisture assessment a challenge for traditional methods. Therefore, researchers are increasingly turning to high-precision full waveform inversion (FWI) to address these limitations. Jazayeri *et al* noted that FWI improved ray-based concrete permittivity and conductivity estimates (Jazayeri *et al* 2019). Xie *et al* correlated the concrete permittivity with its moisture content, and applied FWI to monitor the moisture content variation to detect the setting state of cement paste (Xie *et al* 2022).

To enhance accuracy in moisture detection within concrete structures, the FWI frequently utilizes layered models to more precisely characterize the physical properties of distinct concrete layers. Layered models assume a medium that is horizontally uniform but vertically heterogeneous, an approach widely used in geological surveys, pavement assessments, and concrete dam evaluations (Al-Qadi and Lahouar 2005, Annan 2005, Bigman and Day 2022). This modeling technique not only captures the vertical moisture distribution effectively but also reduces the number of inversion parameters, thereby partially alleviating computational demands. Consequently, moisture profiles in concrete can be mapped by determining the moisture content within each layer of the model.

This paper presents an innovative GPR detection method for concrete moisture content profile. In this paper, the concrete layered model is realized by using the metal with strong electromagnetic reflection as the depth anchor of the concrete moisture content profile. The moisture content of concrete above metal at different depths was quantitatively evaluated by FWI. The GPR detection of the concrete moisture content profile is realized by associating the moisture content at different depths with the depth information.

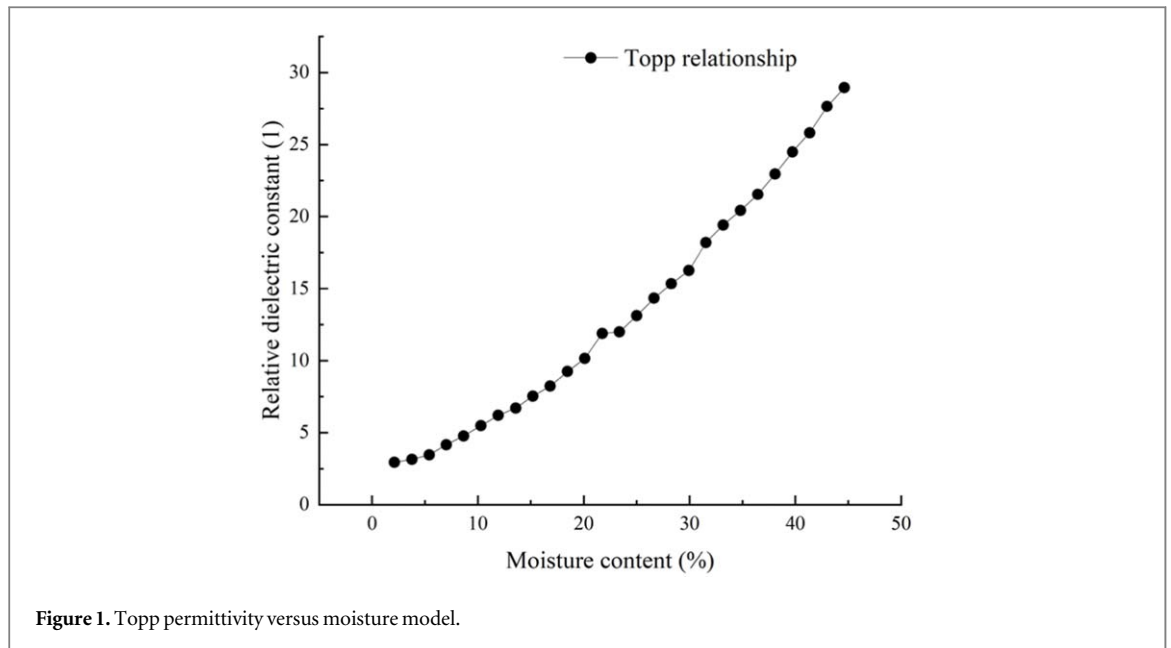


Figure 1. Topp permittivity versus moisture model.

Table 2. Parameters of the concrete.

Parameters	$K_{cw}$	$K_{fw}$	$K_{solid}$	$K_{air}$	$\alpha$
Values	4	82	4	1	0.5

## 2. Detection mechanism

### 2.1. The relationship between moisture content and dielectric constant

Concrete, defined as a mixture of a certain proportion of water, cement, sand and gravel conserved in a given environment. Concrete is a type of composite material. The relative dielectric constant of composite material can be calculated by combining the relative dielectric constant of its components according to its empirical formula. Birchack's theory can be used to compute the relative dielectric constant of composite materials (Birchak *et al* 1974). Based on Birchack's theory, the relative dielectric constant of cement paste can be calculated using equations (1) and (2):

$$K^\alpha = \theta_1 K_{fw}^\alpha + \theta_2 K_{cw}^\alpha + \theta_3 K_{solid}^\alpha + \theta_4 K_{air}^\alpha \quad (1)$$

$$\theta_1 + \theta_2 + \theta_3 + \theta_4 = 1 \quad (2)$$

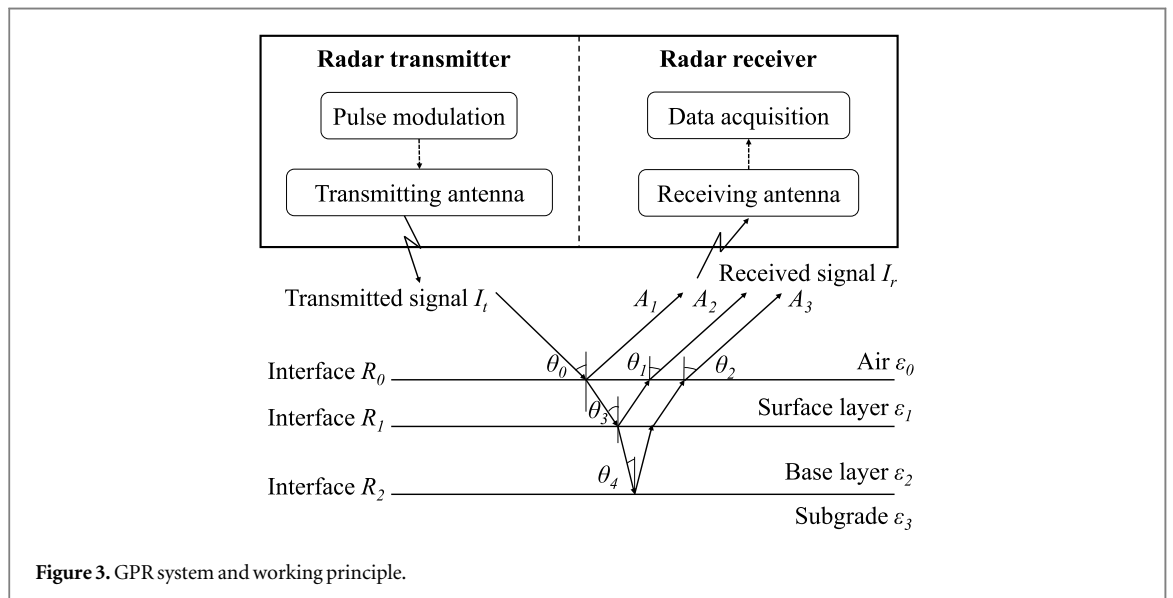
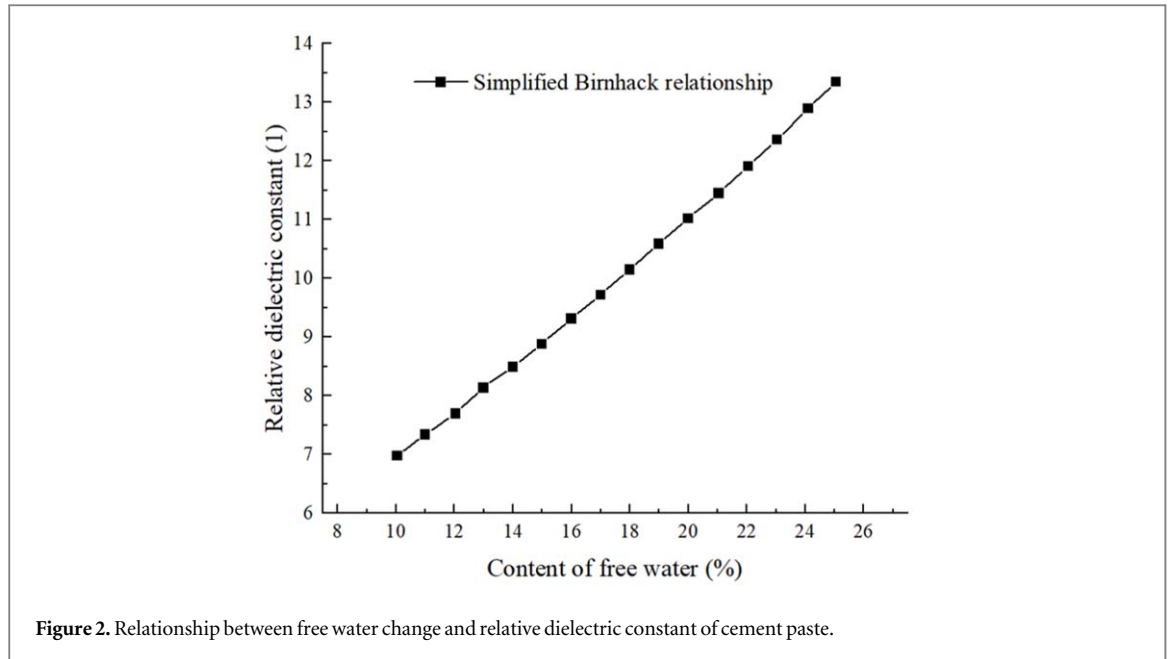
The relative dielectric constants of concrete materials are shown in table 2:

Where  $K_{cw}$ ,  $K_{fw}$ ,  $K_{solid}$  and  $K_{air}$  are the relative dielectric constant of free water, bound water, cement gels, and air, respectively.  $\alpha$  is an experimentally determined value of 0.5. This Alpha coefficient is pre-selected and has been widely accepted by scholars (Birchak *et al* 1974, Dirksen and Dasberg 1993, Sun 2008). Existing researchers have optimized the parameters for data, and now the Alpha coefficients of the permittivity of Birchak's mixing theory model are all 0.5.

The homogeneity of concrete significantly influences the propagation of electromagnetic waves. This study focuses on cases where the inhomogeneity of concrete is relatively minor. Under such conditions, the dielectric constants of coarse aggregates, fine aggregates, and sand are all approximately 4 and can thus be treated as uniform. However, water has a significantly higher relative dielectric constant of 82, making the moisture content the primary factor affecting the electromagnetic properties of concrete structures.

In practical engineering applications, the cost of quantitatively analyzing the specific composition of concrete often exceeds that of the material itself. Hence, simplified empirical formulas are commonly used to estimate concrete's relative dielectric constant. The Topp relationship, derived from experimental data, illustrates the correlation between moisture content and relative dielectric constant, as shown in figure 1, highlighting the essential role of moisture (Topp *et al* 1980).

Free water plays a major role in calculating the relative dielectric constant of concrete. To highlight the effect of free water, we can divide concrete into two parts: free water and other components. The calculation formula



of the relative dielectric constant of concrete is shown in equation (3).

$$K^\alpha = \theta_1 K_{fw}^\alpha + \theta_5 K_{other}^\alpha \tag{3}$$

$$\theta_1 + \theta_5 = 1 \tag{4}$$

In equations(3)–(4),  $K_{other}$  and  $\theta_5$  are the relative dielectric constant and volume fraction of other components, respectively. The relationship between the relative dielectric constant of concrete and the free water content, as derived from equation (3), is depicted in figure 2. We can use the relative dielectric constant change to describe the moisture content change. The change in the relative dielectric constant of the concrete profile is monitored using GPR to produce a gradient map of moisture distribution in this work.

### 2.2. GPR principle

The GPR system comprises a radar control unit and transmitter-receiver antennas. The operational workflow of this equipment is illustrated in figure 3.

As illustrated in figure 3, the propagation pattern of rays reflecting at the interfaces of a homogeneous layer is given by using Maxwell equations with Snell Law.  $\theta_0$ ,  $\theta_3$ , and  $\theta_4$  are the incident angles of an electromagnetic wave incident on each medium stratification plane.  $\theta_1$  and  $\theta_2$  are the incident angles of the electromagnetic wave

on each medium stratification plane.  $A_1$ ,  $A_2$ , and  $A_3$  represent the echo intensity of each layer. Then,  $\varepsilon_0$ ,  $\varepsilon_1$ ,  $\varepsilon_2$ , and  $\varepsilon_3$  refer to the dielectric constant of air, surface layer, base layer, and subgrade, respectively.

GPR modulates high-frequency electromagnetic waves in a solid cavity and then sends them to a dielectric surface by a radiator. Electromagnetic waves penetrate through and reflect on interfaces with different impedances. Engineers can obtain the layer's characteristic information by analyzing time spectrum characteristics and amplitude of the reflected electromagnetic wave signal.

When electromagnetic waves travel through materials with varying dielectric constants, their propagation and reflection behaviors are largely governed by the dielectric contrast between these media. Higher dielectric constants lead to slower wave propagation. Upon encountering a boundary between materials with different dielectric values, partial reflection and transmission occur, with the reflection intensity determined by the dielectric disparity between the two media (Kalluri and Shrivastava 2017).

In GPR detection, the moisture content in concrete significantly affects the characteristics of electromagnetic signals. Higher moisture levels increase dielectric loss, slow down the propagation speed of electromagnetic waves, and cause rapid signal attenuation (Lai 2006, Júnior 2020). Additionally, fluctuations in moisture content can lead to electromagnetic wave polarity instability. In cases of uneven moisture distribution, this polarity asymmetry may impact the reflection and scattering properties of the signal, resulting in irregular reflections or artifacts in radar data. These effects make it challenging to accurately differentiate target signals from noise (Huisman et al 2003).

### 2.2.1. Ray-based approach of GPR inversion

The assumption is that the GPR pulse is plane waves propagating in the far field. The ray-based method determines average permittivity  $\varepsilon_r$  and conductivity  $\sigma$  value. The ray-based approach analysis requires the identification of the positive peaks in the GPR datasets, which are the maximum of each reflection coming from the highly differentiated interfaces. The electromagnetic propagation of the ray-based approach is also included in the GPR system in figure 3.

### 2.2.2. Relative permittivity calculation by ray-based method

The velocity  $v$  in m/ns is calculated by multiplying the two-way travel distance across the element thickness  $2d$  in m by the travel time difference  $t_2 - t_1$  in ns.

$$v = \frac{2d}{(t_2 - t_1)} \quad (5)$$

The speed at which electromagnetic waves propagate through a medium is largely determined by the medium's relative dielectric constant. Therefore, this propagation speed can be directly calculated using the relative dielectric constant in conjunction with the electromagnetic wave velocity in vacuum.

$$v = \frac{c_0}{\sqrt{\varepsilon_r}} \quad (6)$$

where the electromagnetic wave velocity in vacuum  $c_0 = 0.3 \text{ m ns}^{-1}$ . Combined with equations (5) and (6) above, the permittivity can be obtained as:

$$\varepsilon_r = \left( \frac{c_0}{2d} (t_2 - t_1) \right)^2 \quad (7)$$

The travel time difference and amplitude ratio are used in ray-based analysis, which may be applied to raw data. The assumption of a pulse propagating vertically, employed to simplify computations, is around 12% error.

GPR detection of different layers requires substantial electrical differences between media, as shown in equation (8).

$$P_r = \left| \frac{\sqrt{\varepsilon_1} - \sqrt{\varepsilon_2}}{\sqrt{\varepsilon_1} + \sqrt{\varepsilon_2}} \right| \geq 0.01 \quad (8)$$

$P_r$  refers to the commonly used ray-based inversion method in engineering, which requires the minimum difference between two media to be detectable by GPR. The permittivity of two distinct media is represented by  $\varepsilon_1$  and  $\varepsilon_2$ . In the study of this article, the consequences of moisture content differences at various depths on the electrical characteristics of concrete at different depths cannot be directly identified in GPR echo signals. The most widely used ray-based approach in engineering cannot determine the concrete moisture content profile from echo signals. Therefore, we intend to use full waveform inversion with higher inversion accuracy for GPR data.

Ray-based methods assume a simplified, homogeneous model and rely primarily on arrival times to evaluate changes in dielectric constants, limiting their ability to capture small-scale dielectric disturbances due to moisture fluctuations. In contrast, FWI incorporates time, amplitude, and phase information, enhancing inversion constraints and reducing model uncertainty. By accurately aligning with actual waveforms, FWI offers a more precise assessment of the spatial characteristics of non-uniform moisture distributions, particularly in regions with heterogeneous moisture content.

### 2.3. Full waveform inversion of GPR inversion

Full waveform inversion (FWI) is a data fitting technology originating from seismic data processing, which extracts quantitative information by searching for model parameters most suitable for observed data (Virieux and Operto 2009). The approach incorporates forward modeling, which necessitates an initial model of the material parameters derived from the ray-based method and an estimation of the antenna source wavelets.

#### 2.3.1. Full waveform forward model

Accurate model data is necessary to achieve full waveform inversion that minimizes the mismatch between observed data and model data; hence, calculating the electric field requires an efficient and accurate forward model (Patsia et al 2023). The computation of electrical fields in horizontally stratified material is described in this section. The Green function is used to explain the propagation of electromagnetic waves, which is solved in the horizontal wavenumber-frequency ( $F-K$ ) domain. Convolution of the source wavelet  $W(t)$  with the Green function  $G(t, x)$  yields the time domain electric field  $E(t, x)$  for a point dipole source. In the frequency domain, this operation is equivalent to a multiplication

$$\hat{E}(f, x, m) = \hat{G}(f, x, m) \cdot \hat{W}(f) \quad (9)$$

where  $\hat{\cdot}$  means the corresponding functions in the frequency domain,  $f$  is the frequency,  $x$  is a 3D space variable, and  $m$  represents the characteristics of the medium.

#### 2.3.2. Source wavelet estimation

In commercial GPR systems, the effective source wavelet is unknown and is related to antenna coupling. Therefore, evaluating the effective source wavelet based on the measurement data is necessary. Due to the limited length of the GPR antenna and the point dipole antenna being considered in the forward model of the Green function, the effective source wavelet can be estimated from the data that incorporates the effect of the effective finite length. A Green function  $\hat{G}(f_n, x_m, m)$  can be derived using the medium parameters  $m$ , and an effective source wavelet can be produced by deconvolution of the measured electrical field  $\hat{E}_{obs}(f_n, x_m, m)$  with the Green function  $\hat{G}(f_n, x_m, m)$ . The best effective source wavelet  $\hat{W}_{est}(f_n)$  for a specific frequency  $f_n$  can be obtained by using the least square technique to solve the overdetermined system of equations (Ernst et al 2007). Reference ground penetrating radar measurements place the radar at a fixed height above the metal plate to reconstruct this wavelet (Liu et al 2018). Then spectral division is used to obtain the effective source wavelet from the reference measurement.

$$\hat{G}(f_n, x_m, m) = \hat{W}^{-1}(f_n) \cdot \hat{E}(f_n, x_m, m) \quad (10)$$

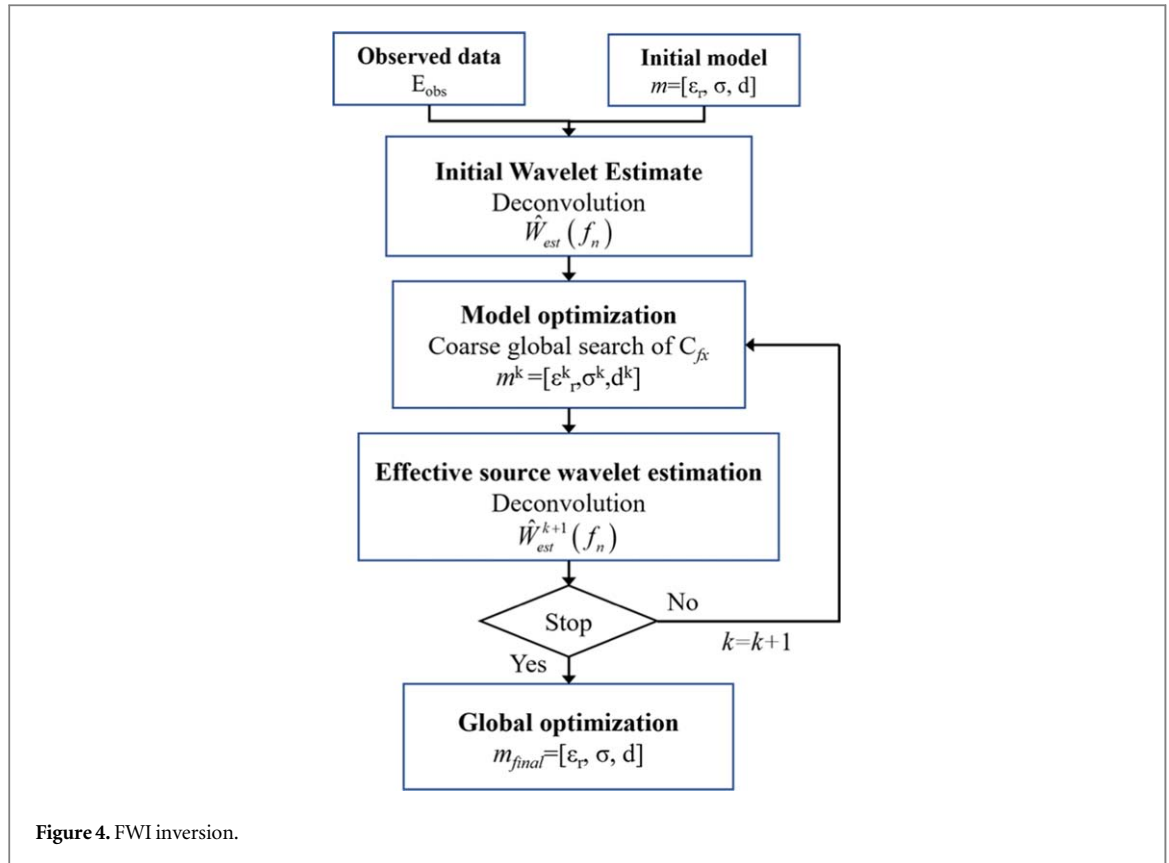
$$\hat{W}_{est}(f_n) = \hat{G}^{-1}(f_n, x_m, m) \cdot \hat{E}_{obs}(f_n, x_m, m) \quad (11)$$

where  $\hat{W}_{est}(f_n)$  is the frequency domain estimation of the source wavelet, and  $\hat{W}(f_n)$  is the default source wavelet to compute the Green function  $\hat{G}(f_n, x_m, m)$  with equation (10).  $x_m$  is the offset of the GPR antenna.

#### 2.3.3. Model optimization

The effectiveness of full waveform inversion is affected by the correctness of the initial model. Using an initial model far from the actual global minimum may result in inaccurate findings due to local minima. We use the inversion value based on the ray-based approach as the starting value of full waveform inversion to improve the robustness of the inversion strategy to the local minimum and ensure convergence to the global minimum that returns the actual value of the electrical characteristics of the concrete. A local optimization algorithm based on the simplex search algorithm is started for each starting model and a local minimum is found. Assume that the local minimum of the minimum cost function is the global minimum.

The synthetic GPR data with configuration parameters was created based on the observed data and modeled using equations (3), (4) and (7) after the initial model was built using the ray-based approach and the effective source wavelet was determined. The mismatch between the observed data and the synthesized data of wave propagation in the frequency domain and time domain is reduced by adjusting the model parameter  $m$ :



$$C_f(m) = \frac{1}{M} \frac{1}{N} \sum_{m=1}^M \sum_{n=1}^N |\hat{E}_{obs}(f_n, x_m) - \hat{G}(f_n, x_m, m) \hat{W}_{est}(f_n)| \quad (12)$$

where  $\hat{E}_{obs}(f_n, x_m)$  is observed data in the frequency domain, and  $M$  is the number of offsets. The number of observed data is denoted by  $N$ .

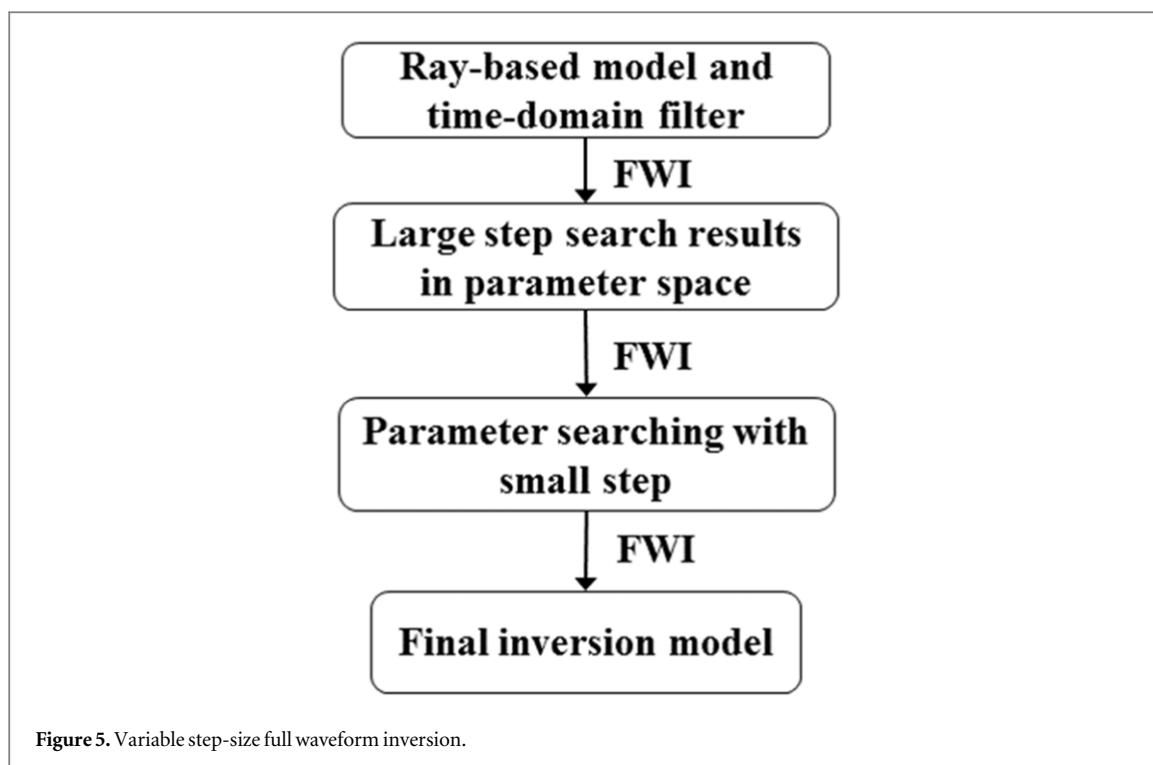
In summary, the data processing flow of full waveform inversion is shown in figure 4.

#### 2.3.4. Ray-based time-domain filters

Focus on grasping the inversion information of the target information, irrelevant information is filtered through the filter to avoid affecting the inversion results (Busch *et al* 2013). Therefore, a time-domain filter is established using the initial model obtained by the ray-based method for each multilayer parameter inversion. To prevent the current layer's inversion from being impacted by the subsequent inaccurate layer's parameter, the time domain filter's effect can filter the data after the target layer. The error of the inversion of some layers caused by the inaccurate parameters of the succeeding layers can be significantly reduced after adding the time-domain filter determined by the initial model of the ray-based method.

#### 2.3.5. Variable step-size full waveform

This research suggests variable step-size full waveform inversion to accelerate the optimization process of full waveform inversion. Variable step-size full waveform inversion can significantly improve the inaccuracy of inversion results caused by large deviations of initial model results, which leads to the need to enlarge the search space of parameter inversion to avoid falling into the local minimum. The variable step-size inversion approach can decrease the amount of calculation while increasing inversion effectiveness. Variable step-size full waveform inversion first adopts a large step size for parameter search in the initial inversion parameter space. Searching the parameter space with a large step can effectively avoid the inversion result falling into the local minimum. Secondly, after obtaining the large-step inversion's parameter results, they are used as the starting point for the small-step full waveform inversion. A higher-precision inversion is carried out in a smaller parameter space with a smaller step, and the final inversion result is obtained through several iterations. The model inversion process is shown in figure 5.



### 3. Simulation

The concrete moisture content profile can be detected if a metal total reflection interface is introduced in the medium with full waveform inversion. The quantitative moisture evaluation of concrete profiles can be accomplished in this article by employing the known steel bar position in concrete combined with full waveform inversion. In this chapter, we intend to use synthetic data to invert multilayer small-difference models to verify this assumption. Figure 6 shows an example of a multilayer medium, whose model parameters are shown in table 3.

To test the multilayer inversion method for detecting the concrete moisture content profile, the comprehensive test considers the typical specific settings corresponding to the scene introduced in figure 6. The multilayer medium model, whose electrical differences are less than the detection requirement of the ray-based method, is modeled in gprMax (Warren *et al* 2016). The GPR receiving antenna and excitation source are simplified to point source models, which can be determined in actual environments using phase center assessment (Lambot *et al* 2004). Different moisture contents at various depths of concrete can be considered medium with various electrical characteristics. Inside, there is an oblique metal cylinder that serves as rebar. The modeling information of each layer's thickness and medium information is the same as in table 3.

The relative dielectric constant of concrete typically ranges from 3 to 12. Moisture distribution over a thickness of 3 cm reflects the diffusion and transport properties of water, providing stable moisture content measurements (Holter and Geving 2016). The thickness of each layer is set to 0.03 m, which means that the resolution of GPR detecting the concrete moisture content profile is 0.03 m.

When GPR uses antennas with different center frequencies, it enhances both the resolution and depth range of detection, allowing for more accurate structural information in complex media. Low frequencies penetrate deeper, suitable for imaging subsurface structures but with limited resolution for finer details (Pipan *et al* 2003). In contrast, high frequencies offer better resolution for detecting subtle geological features but are more susceptible to noise, which can obscure signals in shallow layers (Forte and Pipan 2017). Additionally, high-frequency data inversion demands more computational resources due to increased data volume and complexity (Virieux and Operto 2009). In gprMax, a Ricker wavelet with a center frequency of 2.6 GHz is employed to excite the pulse of the Hertzian dipole antenna, achieving a balance between accuracy and penetration depth. Perfect matching layer (PML) absorption is employed to avoid reflection at the border. The distance between the transmitter and receiver is fixed at 0.05 m.

The metal reflection interface, modeled as a rebar, simulates real reinforced concrete structures, where metal rebars enable GPR to assess moisture by reflecting signals. The multilayer model with incremental moisture variations represents typical moisture distribution across concrete depths due to environmental factors, with the 3 cm layer thickness reflecting practical GPR resolution. The 2.6 GHz Ricker wavelet provides an effective

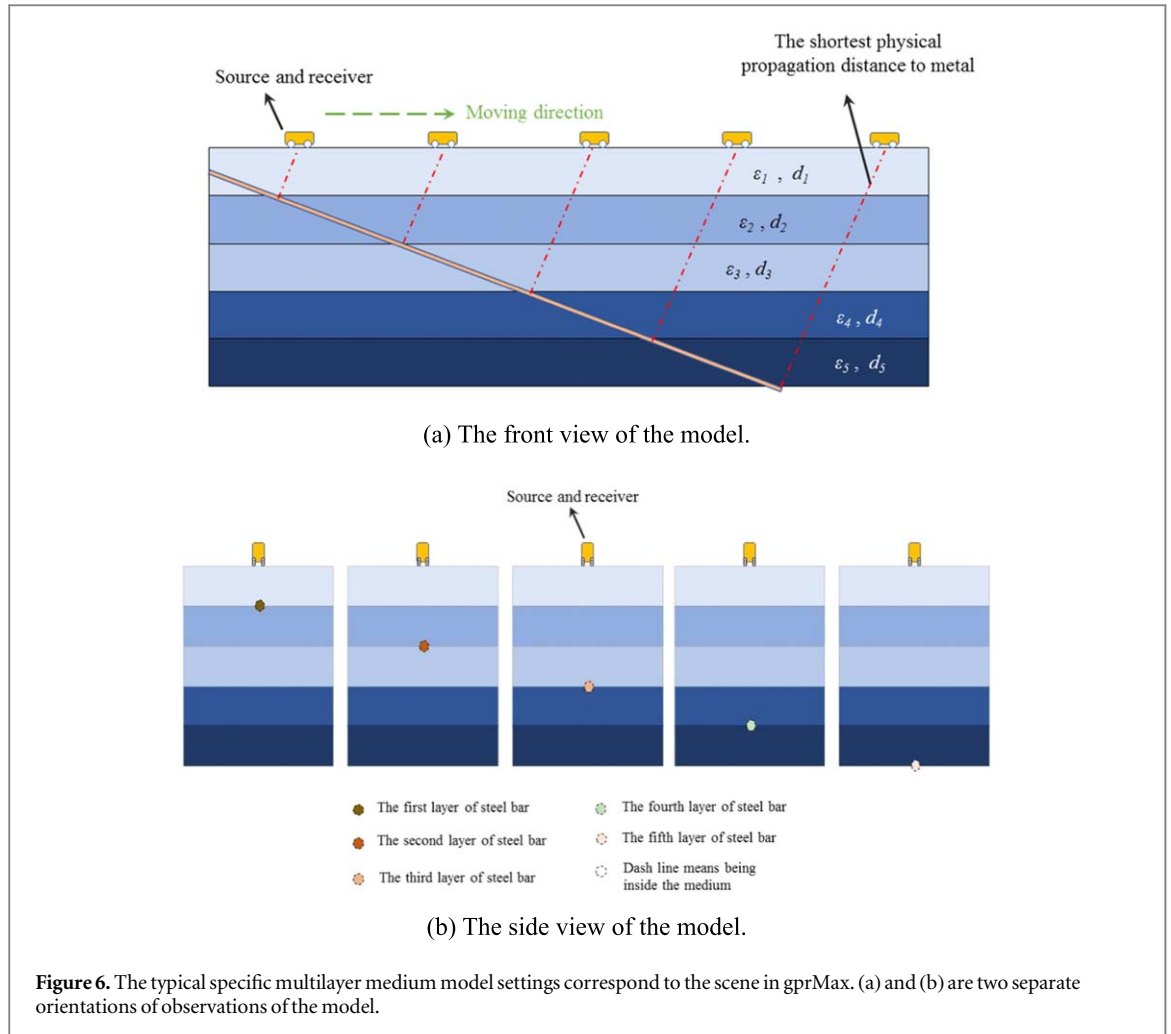


**Table 3.** Thickness and medium information of the multilayer model.

Position	Permittivity	Thickness ( <i>m</i> )
1 <sup>th</sup> layer	4.72	0.03
2 <sup>nd</sup> layer	5.22	0.03
3 <sup>rd</sup> layer	6.15	0.03
4 <sup>th</sup> layer	6.52	0.03
5 <sup>th</sup> layer	5.93	0.03

balance of depth penetration and resolution, while the 0.05 m transmitter-receiver spacing matches standard equipment setups. The PML boundaries minimize reflections, simulating open boundaries. This setup enables the effective use of both ray-based and full waveform inversion methods for determining the moisture content profile, as the metal rebar provides a reliable reflective interface for analyzing the relative dielectric properties of each layer.

The medium underneath the metal does not affect the echo information since it is an electromagnetic total reflection surface. The electrical information of the medium at various depths is derived by combining metal echo information from various depths with full waveform inversion, which determines the concrete moisture content profile. The ray-based method can obtain comprehensive information about the medium at different depths. The ray-based result is used as the initial model of full waveform inversion.

The following is a ray-based calculation example. Figure 7 shows the echo information of rebars at different distances in multilayer media. Since the depth of the rebar is known, we use the travel time of the electromagnetic wave reflected from the rebar to calculate the relative dielectric constant of different dielectric layers.

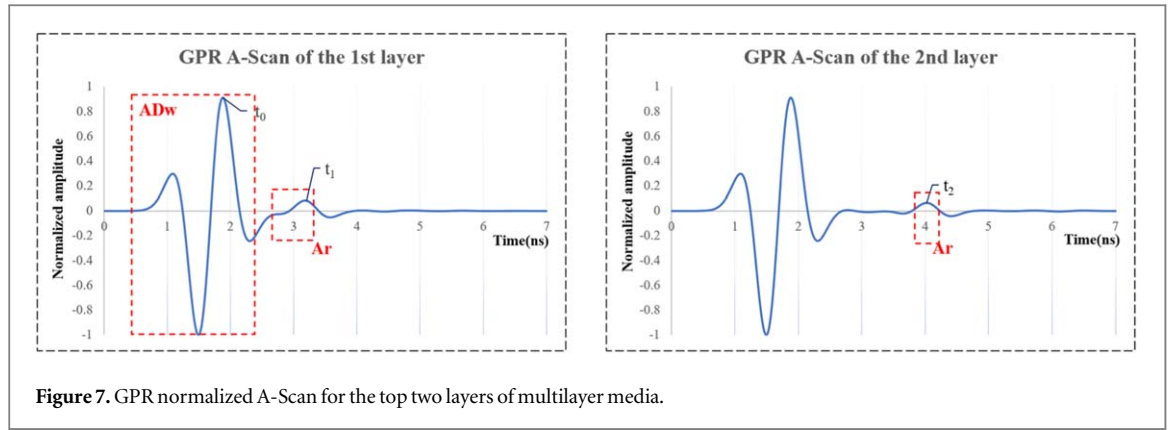


Figure 7. GPR normalized A-Scan for the top two layers of multilayer media.

Table 4. Ray-based inversion model.

Position	Permittivity	Actual permittivity
1 <sup>th</sup> layer	3.24	4.72
2 <sup>nd</sup> layer	4.12	5.22
3 <sup>rd</sup> layer	5.10	6.15
4 <sup>th</sup> layer	7.34	6.52
5 <sup>th</sup> layer	5.01	5.93

In the simulation, the absence of noise allows for calculating the relative dielectric constant  $\varepsilon_1$  of the initial layer. This is achieved by utilizing the time difference between the direct wave (ADw),  $t_0$ , and the reflected wave (Ar),  $t_1$ , at the base of the first layer:

$$\varepsilon_1 = \left( \frac{c_0}{2d} (t_1 - t_0) \right)^2 \quad (13)$$

Subsequently, the relative dielectric constant  $\varepsilon_2$  of the second layer can be determined by employing the time of the reflected wave at the base of the first layer,  $t_1$ , and the time of the reflected wave at the base of the second layer,  $t_2$ :

$$\varepsilon_2 = \left( \frac{c_0}{2d} (t_2 - t_1) \right)^2 \quad (14)$$

The calculation of subsequent layers is the same as above. Therefore, we can get the initial ray-based model, as shown in table 4 below.

The concrete profile is stratified according to the initial model created using the ray-based approach, so that the inversion can achieve convergence in fewer iterations and save computation time. The medium information of the first layer is obtained by combining the echo information of the first layer of metal reflection with full waveform inversion. Then the information of the following layers is further inverted. When inverting the second layer of medium information, the first layer of inversion medium information can be utilized as *a priori* information to perform full waveform inversion from top to bottom.

The ray-based initial model can offer time-domain filters for various layers in multilayer full waveform inversion to lessen the impact of the succeeding layers of the metal reflector in the initial model on the inversion outcomes. The function of the time domain filter is to ensure that the trace information of full waveform inversion in different layers only contains the echo information above the target layer and the target layer, so as to avoid the electromagnetic wave diffraction interference from the information below the target layer.

The initial effective source wavelet is assessed based on the approximation of far-field rays. The global search and local minimization of the combination is the straightforward approach for updating the initial model parameter  $m$ . The global search is carried out by calculating the objective function  $C_f$  at each grid point of the equidistant grid of  $m$  in the interval  $[m - \alpha_0 m, m + \alpha_0 m]$ , where  $\alpha_0$  is the specified percentage deviation relative to the initial model.

The relative deviation of the initial ray-based model is large, and the parameter search space is relatively large. Based on the principle of variable step-size full waveform inversion, we use a larger step to search the target model, which can be used as the initial value of the model for small parameter space inversion. The final

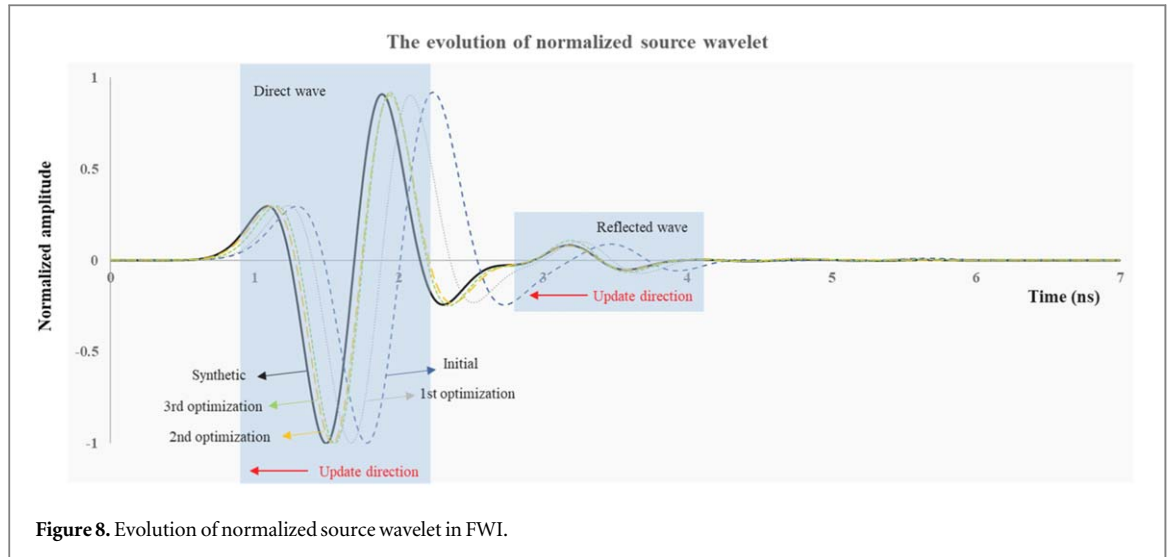


Figure 8. Evolution of normalized source wavelet in FWI.

Table 5. Three groups of different initial multilayer model.

Initial permittivity	Initial model 1	Initial model 2	Initial model 3
1 <sup>th</sup> layer	3.24	3.54	3.04
2 <sup>nd</sup> layer	4.12	4.01	4.30
3 <sup>rd</sup> layer	5.10	5.22	4.92
4 <sup>th</sup> layer	7.34	7.04	7.67
5 <sup>th</sup> layer	5.01	5.30	4.71

optimization result is then obtained by performing a small-step, high-precision inversion of the parameter small space using the model value obtained in the previous step.

Three groups of different initial models are set to study the stability and convergence performance of the method by randomly shifting the initial values of the ray-based model by about 15%, as shown in table 5 below.

The strong link between the initial model and the source wavelet necessitates a new estimation of the effective source wavelet after optimizing the model parameters. Therefore, the Green function is calculated for the optimized parameter  $m$ , and the new estimated source wavelet  $\hat{W}_{est}(f_n)$  is obtained through deconvolution equation (9). The updated estimation wavelet and the optimized model attributes are utilized as the starting value for the following iteration. This approach is continued until the objective function equation (10) fulfills the termination condition  $C_f(m^k) > C_f(m^{k-1})$ . Figure 8 shows the evolution of the source wavelet in the full waveform inversion.

Figure 8 illustrates the iterative process of the A-Scan from the initial model toward the true model. The optimal results for each iteration are plotted in figure 8. During each iteration, the waveform of the direct wave and target reflection wave progressively approaches the true waveform. After the third iteration, the phase and amplitude of the waveform closely match the true waveform, indicating that the current inversion model can be regarded as the identified true model.

Through the variable step-size full waveform inversion method, the parameter searching of large space and large step can obtain the initial value  $m$  of the model, which is close to the actual value of the simulation. Then, after the parameter searching of small space and a small step near the above model value, the final inversion value of the model can be obtained by iterative inversion. The results for each step are shown in tables 6 and 7 below.

From table 7, it can be observed that although the initial models differ, the results ultimately converge to values that are close to the actual measured values. In the absence of noise, the maximum simulation inversion error is 0.33%. The evolution of parameters also verifies that the full waveform inversion method has good convergence and stable performance.

## 4. Experiments

### 4.1. Experimental scheme and design

The gravimetric method (GM) is one of the most common measurements of moisture content testing method, which is used as a calibration to compare GPR measurement results in the experiment. To verify the portability



Figure 9. Mortar and concrete test blocks.

Table 6. FWI results with large-step search.

Permittivity	Model 1	Model 2	Model 3	Actual permittivity
1 <sup>th</sup> layer	4.80	4.80	4.79	4.72
2 <sup>nd</sup> layer	5.19	5.20	5.23	5.22
3 <sup>rd</sup> layer	6.02	6.04	6.00	6.15
4 <sup>th</sup> layer	6.58	6.56	6.60	6.52
5 <sup>th</sup> layer	5.81	5.94	5.93	5.93

Table 7. FWI final inversion results.

Inversion result	Actual permittivity	Model 1		Model 2		Model 3	
		Permittivity	Error	Permittivity	Error	Permittivity	Error
1 <sup>th</sup> layer	4.72	4.72	0	4.72	0	4.72	0
2 <sup>nd</sup> layer	5.22	5.23	0.19%	5.23	0.19%	5.23	0.19%
3 <sup>rd</sup> layer	6.15	6.14	0.16%	6.14	0.16%	6.14	0.16%
4 <sup>th</sup> layer	6.52	6.52	0	6.52	0	6.52	0
5 <sup>th</sup> layer	5.93	5.91	0.33%	5.93	0	5.93	0

and universality of the GPR measurement method, two materials commonly used in engineering, including mortar and concrete, are tested in this paper. Meanwhile, the profiles of two widely used materials are consistent with the simulation model to verify the simulation results and FWI method.

This article used ordinary Portland cement (OPC) to make mortar and concrete for experiments. The particle size of the sand is between 8–16 mm. The diameter of the concrete aggregate does not exceed 3 cm, which is the thickness of each concrete block. Each experimental group consists of five layers of  $15 \times 15 \times 3 \text{ cm}^3$  samples of the same material, but the moisture content of each layer of samples is different. The experimental samples of two groups of different materials are shown in figure 9 below.

The GPR instrument is shown in figure 10 above. The method of FWI necessitates a suitable measurement height and a consistent distance between each measurement. This study utilizes the SIR-4000 ground penetrating radar, equipped with a 2600 MHz operational antenna, to assess the profiles of mortar and concrete, each with varying moisture content levels. Since it is difficult to measure the standard moisture content if the rebar is directly placed inside the materials, the metal plate is adopted as the full reflective surface to replace the role of the rebar. In the subsequent research, attempts will be considered to combine the distribution of rebars in construction to research the inversion of the moisture content of the concrete dam profile.

In the concrete inspection region, metal plates with varying depths and fixed spacing are pre-embedded as calibration reflection layers. The depth and spacing information of these metal layers serve as prior calibration data for moisture content measurements. The arrangement of metal reflective layer is shown in figure 11.



Figure 10. GPR Experiment measurement.

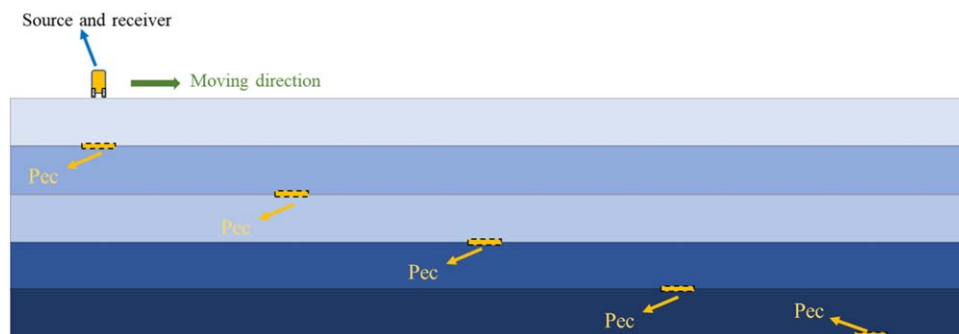


Figure 11. Arrangement of metal reflective layer.

Consequently, this study manipulates the location of the full reflecting surface by methodically positioning a metal plate from the top downwards. This approach is employed to substantiate the feasibility of utilizing full waveform inversion for inverting the concrete moisture content profile.

Due to the difficulty in controlling and calibrating the measurement of moisture content variations in fully cast concrete, this study employs layered casting of test specimens with different moisture contents. This approach allows the use of the gravimetric method to measure the standard moisture content of each layer. Additionally, metal plates commonly used in pavement detection are utilized as reference surfaces (Grote *et al* 2005, Plati and Loizos 2013, De Coster *et al* 2018). In this experiment, metal plates are employed as reflective anchors for each layer. By adjusting the position of the metal plates within the layered model, tests are conducted to simulate reflective anchors at various depths.

The change diagram of the metal reflector during GPR measurement is shown in figure 12 and figure 13. Figures 12 and 13 show a schematic of the variation of the metallic reflector, which is often called the perfect electric conductor (Pec), during GPR measurements.

#### 4.2. Analysis and interpretation of experimental result

Firstly, the moisture contents of each layer of the two experimental groups were measured based on the GM method as the calibration result. Each set of experimental samples will then be measured using GPR, and initial evaluation will be performed using the ray-based approach and then combined with FWI inversion.

##### 4.2.1. Gravimetric method (GM) measurement of moisture content profile

In this experiment, the gravimetric method measurement results of the moisture content profiles of the two groups of experimental samples are shown in table 8 below.

##### 4.2.2. Analysis of GPR measurement of moisture content profile

Each GPR survey records five sets of B-Scan echo data, each containing 50 A-scans. After screening and excluding the abnormal data caused by an abnormal measurement operation, the average value is taken as the

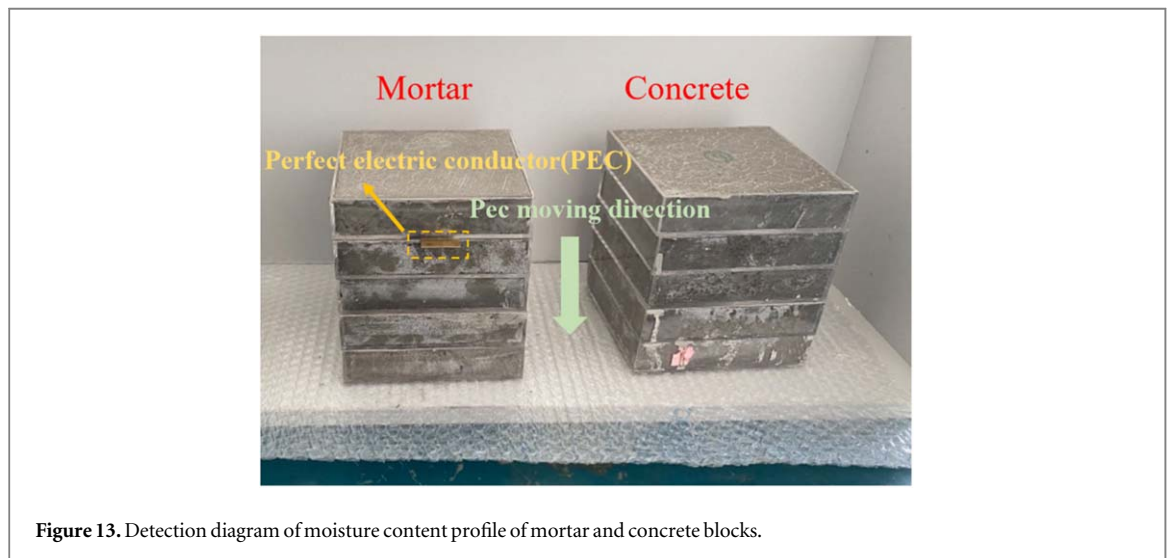
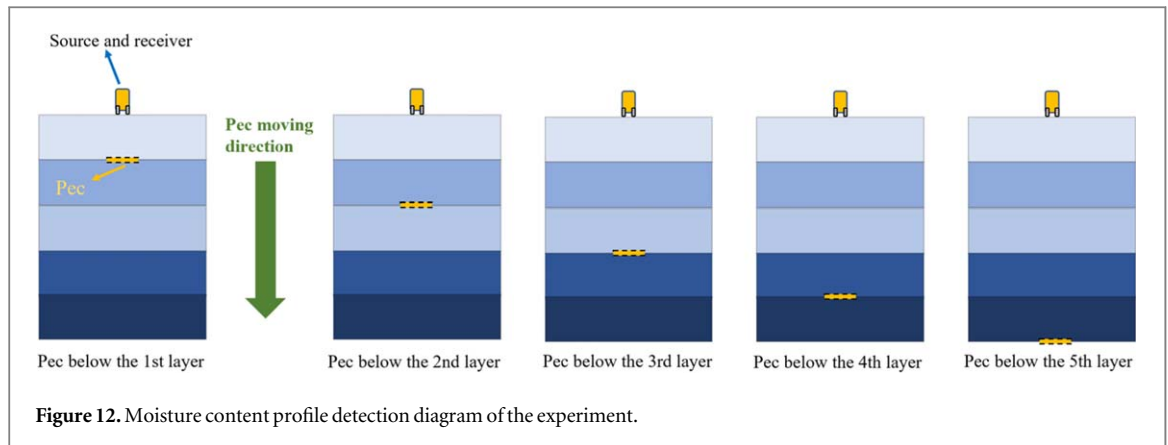


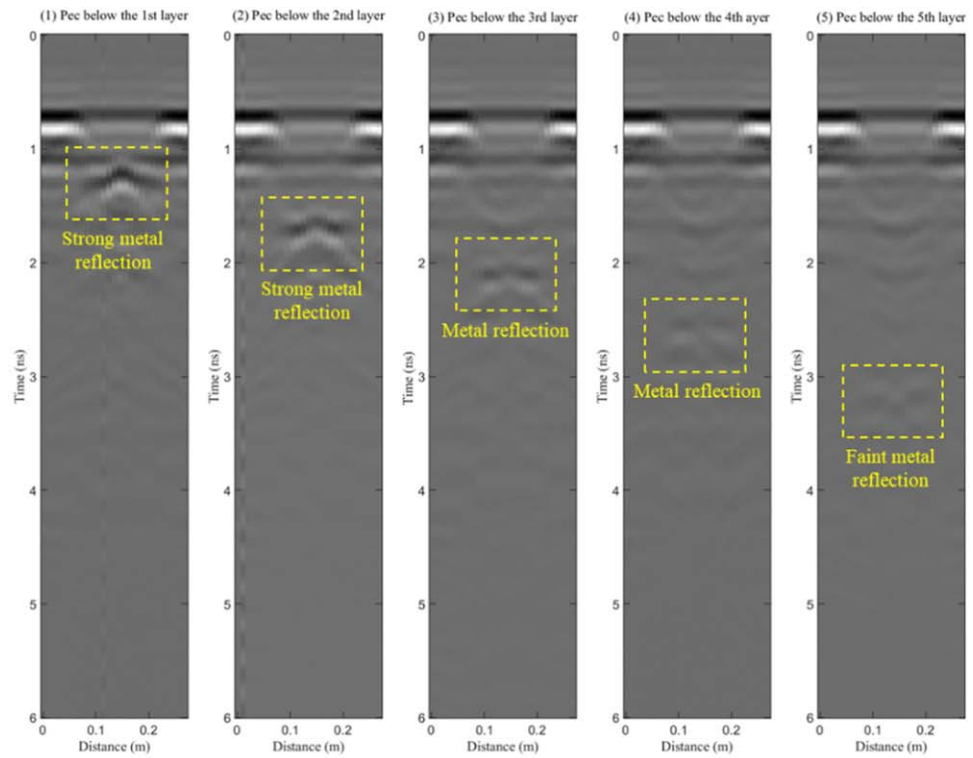
**Table 8.** Results of moisture content profile measured by gravity method.

Layers	Moisture content (%)	
	Mortar	Concrete
1 <sup>st</sup> layer	5.71	4.26
2 <sup>nd</sup> layer	8.39	7.56
3 <sup>rd</sup> layer	11.35	10.86
4 <sup>th</sup> layer	14.05	13.63
5 <sup>th</sup> layer	7.26	9.83

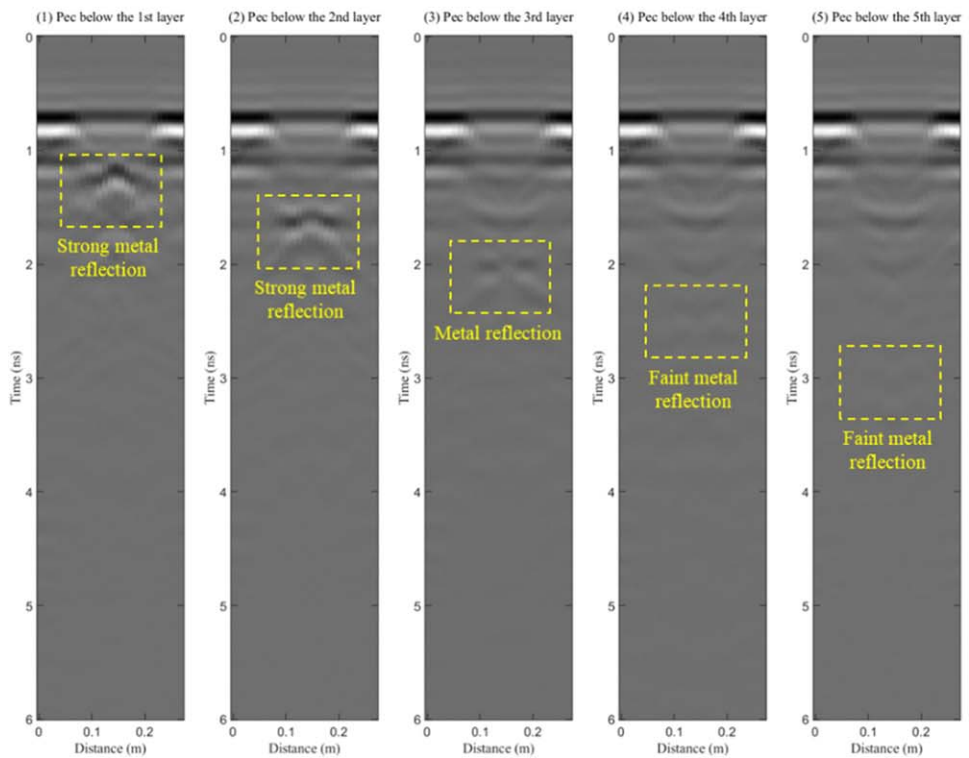
experimental data each time to ensure the universality of the experiment. The final B-Scan measurement data of each group of experimental samples are shown in figure 14.

FWI is usually fitted to raw data without applying linear gain. Metal reflections lacking linear gain are less prominent. As shown in figure 14, the metal reflection points are highlighted with yellow boxes. It can be observed that the reflection intensity of the metal decreases with increasing depth in both concrete and mortar. Because mortar has higher conductivity than concrete, it causes greater electromagnetic wave attenuation (Azarsa and Gupta 2017). Therefore, when the PEC is located below the third layer, the reflections of metals in mortar will be weaker compared to concrete.

Initially, upon identifying the location of the metal full reflector, a ray-based methodology can be employed to estimate the preliminary moisture content profile for each set of experimental samples. This ray-based methodology capitalizes on the propagation velocity of electromagnetic waves in samples with varying moisture content to invert the material's relative dielectric constant. Subsequently, the moisture content profile is



(a) GPR B-Scan measurement of PEC at different layers of concrete blocks.



(b) GPR B-Scan measurement of PEC at different layers of mortar blocks.

**Figure 14.** B-Scan measurement for GPR. (a) and (b) are PEC at different layers of concrete and mortar blocks.

obtained based on the aforementioned linear relationship between the relative dielectric constant and moisture content. The initial model evaluated based on the ray-based method is shown in table 9 below.

Predicated on the initial model evaluated via the velocity ray-based method, a global minimum search is conducted within the parameter space using a large step. This goal is designed to circumvent potential local

**Table 9.** Initial evaluation of the ray-based model in two experimental groups.

Concrete ray-based result	Permittivity	Moisture content (%)
1 <sup>th</sup> layer	6.81	8.65
2 <sup>nd</sup> layer	5.48	4.82
3 <sup>rd</sup> layer	7.08	9.37
4 <sup>th</sup> layer	6.68	8.28
5 <sup>th</sup> layer	5.00	3.32
Mortar ray-based result		
1 <sup>th</sup> layer	6.42	7.57
2 <sup>nd</sup> layer	7.59	10.69
3 <sup>rd</sup> layer	9.59	15.54
4 <sup>th</sup> layer	7.18	9.63
5 <sup>th</sup> layer	4.98	3.29

**Table 10.** FWI results with large-step search of two experimental groups.

Concrete blocks	Permittivity	Moisture content (%)
1 <sup>th</sup> layer	5.75	5.63
2 <sup>nd</sup> layer	7.25	9.82
3 <sup>rd</sup> layer	6.84	8.73
4 <sup>th</sup> layer	7.61	10.75
5 <sup>th</sup> layer	5.83	5.89
Mortar blocks		
1 <sup>th</sup> layer	5.49	4.85
2 <sup>nd</sup> layer	7.42	10.26
3 <sup>rd</sup> layer	8.16	12.14
4 <sup>th</sup> layer	7.42	10.26
5 <sup>th</sup> layer	5.58	5.13

**Table 11.** FWI final results of two experimental groups.

Concrete blocks	Permittivity	Moisture content (%)
1 <sup>th</sup> layer	5.79	5.74
2 <sup>nd</sup> layer	7.08	9.37
3 <sup>rd</sup> layer	6.96	9.04
4 <sup>th</sup> layer	7.75	11.12
5 <sup>th</sup> layer	6.21	6.96
Mortar blocks		
1 <sup>th</sup> layer	5.32	4.34
2 <sup>nd</sup> layer	7.29	9.92
3 <sup>rd</sup> layer	8.62	13.26
4 <sup>th</sup> layer	7.87	11.42
5 <sup>th</sup> layer	5.30	4.28

minima, which may manifest as period jump phenomena in FWI (Virieux and Operto 2009). The FWI inversion results of the large-step search are shown in table 10 below.

The FWI outcome derived from the large-step search is utilized as the model for the final FWI inversion. Leveraging the linear relationship between the relative dielectric constant of concrete and moisture content, we procured the moisture content profile for the two experimental groups measured by GPR, as demonstrated in table 11 below.

#### 4.2.3. Data comparison of measurement results

The final measurement results of GM and GPR are shown in table 12. The average results of each measurement are shown below:

In order to show the difference more clearly between GM and GPR results, the above data are drawn as shown in figure 15 below:

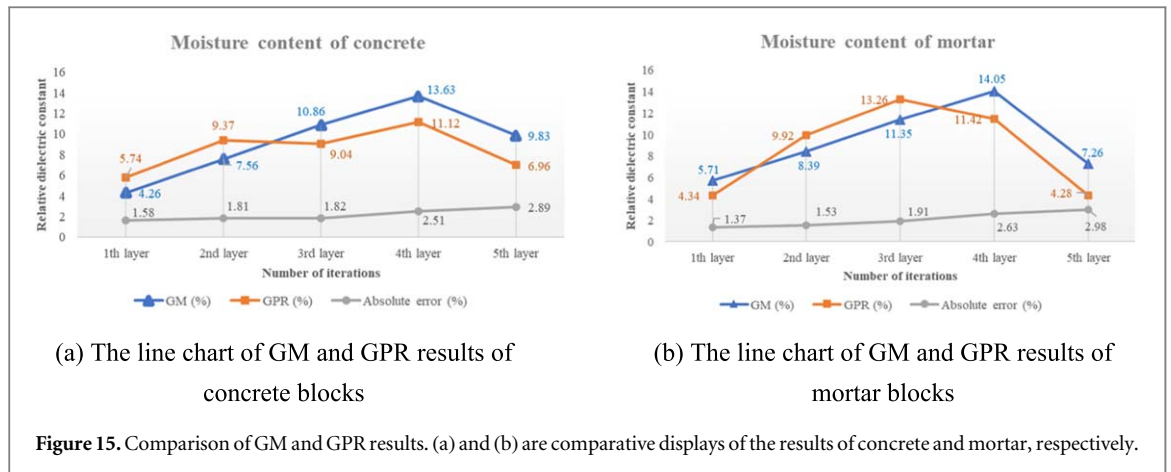


**Table 12.** Comparison of measurement results of GM and GPR.

Parameter	Moisture content of concrete			Moisture content of mortar		
	GM (%)	GPR (%)	Absolute error (%)	GM (%)	GPR (%)	Absolute error (%)
1 <sup>th</sup> layer	4.26	5.74	1.58	5.71	4.34	1.37
2 <sup>nd</sup> layer	7.56	9.37	1.81	8.39	9.92	1.53
3 <sup>rd</sup> layer	10.86	9.04	1.82	11.35	13.26	1.91
4 <sup>th</sup> layer	13.63	11.12	2.51	14.05	11.42	2.63
5 <sup>th</sup> layer	9.83	6.96	2.89	7.26	4.28	2.98
Average error (%)	/	/	2.122	/	/	2.084

While there are some discrepancies in the results obtained from the two methodologies, the trend of moisture content alteration aligns fundamentally with that of the GPR and gravimetric methods. However, the results of each layer moisture content will have a certain error; the maximum absolute error is close to 3%, and the average error is less than 2.5%. Throughout the measurement process, the distribution of moisture content within a singular material plate is not entirely homogeneous, and the presence of data noise can potentially influence the ultimate inversion outcome. This leads to a certain deviation in the inversion of the relative dielectric constant, thereby affecting the inversion of moisture content. The GPR measurement method employed in this study is an initial exploration, and future research will continue to delve into the potential of GPR inversion of moisture content profiles, considering the distribution of rebars under actual working conditions.

In concrete structures, long-term compression, misalignment, and bending of reinforcement can cause variations in the reflection information from metal surfaces. This study assumes that the depth information is known; however, as concrete deteriorates, inaccuracies in depth measurements may occur, leading to errors in the inversion of the dielectric constant. Therefore, simultaneously determining the depth information is essential and will be an important direction for future research.

In practical engineering applications, noise is indeed an unavoidable factor that can interfere with and reduce the recognizability of target signals. Therefore, when applied to real-world scenarios, measures must be taken to eliminate or mitigate noise interference. When the target signal reflection is weak, the use of an averaging method to filter out direct waves is recommended to further improve the signal-to-noise ratio (SNR) of the target reflection. Additionally, considering that noise is uniformly distributed across all frequency bands while target reflections exhibit specificity, background subtraction proves to be an effective method.

## 5. Conclusion

This paper presents a novel method for detecting the concrete moisture content profile using GPR with full waveform inversion.

- The method exploits the linear relationship between the relative dielectric constant and the moisture content of concrete, and uses a metal plate as a full reflector to provide echo information for different layers.

- The method is tested on synthetic and experimental data of mortar and concrete blocks with different moisture contents.

The results show that the method can effectively invert the moisture content profile of concrete with an average error of less than 2.5% compared to the gravimetric method. The method has potential applications in monitoring the hydration state, setting state and strength development of concrete in engineering.

Future research will involve testing this method in real-world engineering cases involving concrete structures in bridges and buildings to confirm its effectiveness in complex field environments, thereby enhancing its reliability for engineering applications. In using FWI for moisture estimation, errors typically stem from model assumptions, data noise, and boundary conditions. An average error below 2.5% is generally acceptable for most engineering needs, while errors exceeding 5% could compromise accuracy, particularly in high-precision contexts.

To improve inversion results, future studies intend to adopt a graded frequency approach, progressing from low to high frequencies, to achieve precise moisture distribution estimates across both shallow and deep layers. Although the current method relies on PEC reflectors, its principles can be extended to other high-dielectric materials, such as TiO<sub>2</sub> ceramics. Developing reflectors suited to field conditions would further support engineering applications by providing reference data that enable easier error quantification and correction in field assessments.

## Acknowledgments

Funding: This study was first funded by National Key R&D Program of China (Grant No. 2022YFC3801100). This research was funded by the National Natural Science Foundation of China (Grant Nos. 52178298 and 52078375).

## Data availability statement

All data that support the findings of this study are included within the article (and any supplementary files).

## ORCID iDs

Zihan Xia  <https://orcid.org/0000-0002-8561-6116>

Liyu Xie  <https://orcid.org/0000-0001-5777-0645>

Peng Zhu  <https://orcid.org/0000-0002-8610-119X>

## References

- Agred K, Klysz G and Balayssac J-P 2018 Location of reinforcement and moisture assessment in reinforced concrete with a double receiver GPR antenna *Constr. Build. Mater.* **188** 1119–27
- Al-Qadi I L and Lahouar S 2005 Measuring layer thicknesses with GPR—theory to practice *Constr. Build. Mater.* **19** 763–72
- Annan A P 2005 GPR methods for hydrogeological studies *Hydrogeophysics* (Springer)
- Azarsa P and Gupta R 2017 Electrical resistivity of concrete for durability evaluation: a review *Adv. Mater. Sci. Eng.* **2017** 8453095
- Bigman D P and Day D J 2022 Ground penetrating radar inspection of a large concrete spillway: a case-study using SFCW GPR at a hydroelectric dam *Case Studies in Construction Materials* **16** e00975
- Birchak J R, Gardner C G, Hipp J E and Victor J M 1974 High dielectric constant microwave probes for sensing soil moisture *Proc. IEEE* **62** 93–8
- Busch S, Van Der Kruk J and Vereecken H 2013 Improved characterization of fine-texture soils using on-ground GPR full-waveform inversion *IEEE Trans. Geosci. Remote Sens.* **52** 3947–58
- De Coster A, Van Der Wielen A, Grégoire C and Lambot S 2018 Evaluation of pavement layer thicknesses using GPR: a comparison between full-wave inversion and the straight-ray method *Constr. Build. Mater.* **168** 91–104
- Dinh K, Gucunski N, Kim J and Duong T H 2016 Understanding depth-amplitude effects in assessment of GPR data from concrete bridge decks *NDT & E International* **83** 48–58
- Dirksen C and Dasberg S 1993 Improved calibration of time domain reflectometry soil water content measurements *Soil Sci. Soc. Am. J.* **57** 660–7
- du Plessis A and Boshoff W P 2019 A review of x-ray computed tomography of concrete and asphalt construction materials *Constr. Build. Mater.* **199** 637–51
- Ernst J R, Green A G, Maurer H and Holliger K 2007 Application of a new 2D time-domain full-waveform inversion scheme to crosshole radar data *Geophysics* **72** J53–64
- Fernandes F M, Fernandes A and Pais J 2017 Assessment of the density and moisture content of asphalt mixtures of road pavements *Constr. Build. Mater.* **154** 1216–25
- Forté E and Pipan M 2017 Review of multi-offset GPR applications: data acquisition, processing and analysis *Signal Process.* **132** 210–20

- Ghodoosi F, Bagchi A, Zayed T and Hosseini MR 2018 Method for developing and updating deterioration models for concrete bridge decks using GPR data *Autom. Constr.* **91** 133–41
- Grote K, Hubbard S, Harvey J and Rubin Y 2005 Evaluation of infiltration in layered pavements using surface GPR reflection techniques *J. Appl. Geophys.* **57** 129–53
- Holter K G and Geving S 2016 Moisture transport through sprayed concrete tunnel linings *Rock Mech. Rock Eng.* **49** 243–72
- Hugenschmidt J and Loser R 2008 Detection of chlorides and moisture in concrete structures with ground penetrating radar *Mater. Struct.* **41** 785–92
- Huisman J A, Hubbard S S, Redman J D and Annan A P 2003 Measuring soil water content with ground penetrating radar: a review *Vadose Zone J.* **2** 476–91
- Jazayeri S, Kruse S, Hasan I and Yazdani N 2019 Reinforced concrete mapping using full-waveform inversion of GPR data *Constr. Build. Mater.* **229** 117102
- Joshaghani A and Shokrabadi M 2022 Ground penetrating radar (GPR) applications in concrete pavements *Int. J. Pavement Eng.* **23** 4504–31
- Júnior J T A 2020 *Health Assessment of Concrete Structures with GPR* (PUC-Rio)
- Kalluri D K and Shrivastava R 2017 Reflection and transmission of electromagnetic waves obliquely incident on a relativistically moving uniaxial plasma slab *Principles of Electromagnetic Waves and Materials* (CRC Press)
- Kalogeropoulos A 2012 *Non-Destructive Determination of Chloride and Water Content in Concrete Using Ground Penetrating Radar* (EPFL)
- Kaplanvural I, Pekşen E and Özkap K 2018 Volumetric water content estimation of C-30 concrete using GPR *Constr. Build. Mater.* **166** 141–6
- Klewe T, Strangfeld C, Ritzer T and Kruschwitz S 2021 Combining signal features of ground-penetrating radar to classify moisture damage in layered building floors *Applied Sciences* **11** 8820
- Lai W-L W 2006 Characterization of porous construction materials using electromagnetic radar wave *Ph.D dissertation* Hong Kong Polytechnic University <https://theses.lib.polyu.edu.hk/handle/200/2269>
- Lambot S, Slob E C, Van Den Bosch I, Stockbroeckx B and Vanclooster M 2004 Modeling of ground-penetrating radar for accurate characterization of subsurface electric properties *IEEE Trans. Geosci. Remote Sens.* **42** 2555–68
- Laurens S, Balayssac J, Rhazi J, Klysz G and Arliguie G 2005 Non-destructive evaluation of concrete moisture by GPR: experimental study and direct modeling *Mater. Struct.* **38** 827–32
- Li Z, Zhou X, Ma H and Hou D 2022 *Advanced Concrete Technology* (Wiley)
- Liu T, Klotsche A, Pondkule M, Vereecken H, Su Y and Van Der Kruk J 2018 Radius estimation of subsurface cylindrical objects from ground-penetrating-radar data using full-waveform inversion *Geophysics* **83** H43–54
- Moradillo M K, Reese S R and Weiss W J 2019 Using neutron radiography to quantify the settlement of fresh concrete *Advances in Civil Engineering Materials* **8** 71–87
- Neville A M 1995 *Properties of Concrete* (Longman London)
- Patsia O, Giannopoulos A and Giannakis I 2023 GPR full-waveform inversion with deep-learning forward modelling: a case study from non-destructive testing *IEEE Trans. Geosci. Remote Sens.* **61** 2003910
- Pipan M, Forte E, Guangyou F and Finetti I 2003 High resolution GPR imaging and joint characterization in limestone *Near Surface Geophysics* **1** 39–55
- Plati C and Loizos A 2013 Estimation of *in situ* density and moisture content in HMA pavements based on GPR trace reflection amplitude using different frequencies *J. Appl. Geophys.* **97** 3–10
- Prego F, Solla M, Núñez-Nieto X and Arias P 2016 Assessing the applicability of ground-penetrating radar to quality control in tunneling construction *Journal of Construction Engineering and Management* **142** 06015006
- Shetty M and Jain A 2019 *Concrete Technology (Theory and Practice), 8e* (S Chand Publishing)
- Sugiyama T and Promentilla M A B 2021 Advancing concrete durability research through x-ray computed tomography *J. Adv. Concr. Technol.* **19** 730–55
- Sun Z 2008 Estimating volume fraction of bound water in Portland cement concrete during hydration based on dielectric constant measurement *Mag. Concr. Res.* **60** 205–10
- Topp G C, Davis J and Annan A P 1980 Electromagnetic determination of soil water content: measurements in coaxial transmission lines *Water Resour. Res.* **16** 574–82
- Virieux J and Operto S 2009 An overview of full-waveform inversion in exploration geophysics *Geophysics* **74** WCC1–CC 26
- Voigt T, Sun Z and Shah S P 2006 Comparison of ultrasonic wave reflection method and maturity method in evaluating early-age compressive strength of mortar *Cem. Concr. Compos.* **28** 307–16
- Wang Y, Yuan Q, Deng D, Ye T and Fang L 2017 Measuring the pore structure of cement asphalt mortar by nuclear magnetic resonance *Constr. Build. Mater.* **137** 450–8
- Warren C, Giannopoulos A and Giannakis I 2016 GPRMAX: open source software to simulate electromagnetic wave propagation for ground penetrating radar *Comput. Phys. Commun.* **209** 163–70
- Xie L, Xia Z, Xue S and Fu X 2022 Detection of setting time during cement hydration using ground penetrating radar *Journal of Building Engineering* **60** 105166
- Xue S, Yi Z, Xie L and Wan G 2021 Double-frequency passive deformation sensor based on two-layer patch antenna *Smart Struct Syst* **27** 969–82
- Yi Z, Xue S, Xie L, Wan G and Wan C 2023 Detection of setting time during cement hydration using multi-electromagnetic parameters of patch antenna sensor *IEEE Trans. Instrum. Meas.* **72** 8005909